

Technical Note: Analytical Solution for Well Water Response to Earth Tides in Leaky Aquifers with Storage and Compressibility in the Aquitard

Rémi Valois^{1, 2, *}, Agnès Rivière³, Jean-Michel Vouillamoz⁴, Gabriel C. Rau⁵

¹French Red-Cross, 4 rue Diderot, Paris, France

²Hydrogeology Lab, UMR EMMAH, University of Avignon, 74 rue Louis Pasteur, Avignon, France

³Geosciences Department, Mines Paris - PSL, 75272 Paris, France

⁴Univ. Grenoble Alpes, IRD, CNRS, INRAE, Grenoble INP, IGE, 38000 Grenoble, France

⁵School of Environmental and Life Sciences, The University of Newcastle, Callaghan, Australia

*Correspondence: remi.valois1@gmail.com; Tel.: +33-6-8434-0779 (R.V.)

Key points

- A new analytical solution for Earth tide induced well water level fluctuations in semi-confined aquifers considering aquitard storage, aquitard response to tidal strain, skin and wellbore storage effects is developed
- The solution correctly reflects previously observed but unexplained amplitude-frequency relationships and positive or negative phase shifts
- Diagnostic information about subsurface hydro-geomechanical properties can be derived from amplitude ratio and phase shifts for both semi-diurnal and diurnal tides

Abstract

In recent years, there has been a growing interest in utilizing the groundwater response to Earth tides as a means to estimate subsurface properties. However, existing analytical models have been insufficient in accurately capturing realistic physical conditions. This study presents a new analytical solution to calculate groundwater response to Earth tide strains, including storage and compressibility of the aquitard, borehole storage and skin effects. We investigate the effects of aquifer and aquitard parameters on well water response to Earth tides at two dominant frequencies (O_1 and M_2) and compare our results with hydraulic parameters obtained from a pumping test. Inversion of the six hydro-geomechanical parameters from amplitude response and phase shift of both semi-diurnal and diurnal tides provides relevant information about aquifer transmissivity, storativity, well skin effect, aquitard hydraulic conductivity and diffusivity. The new model is able to reproduce previously unexplained observations of the amplitude and frequency responses. We emphasize the usefulness in developing relevant methodology to use the groundwater response to natural drivers for characterizing hydrogeological systems.

38 1. Introduction

39 Aquifer properties play a vital role in managing groundwater resources, particularly amid increasing
40 anthropogenic groundwater use and the impact of climate change. While pump testing can be costly,
41 there exists a cost-effective alternative for assessing aquifer hydraulic properties - analysing the
42 groundwater response to Earth tides or atmospheric tides (McMillan et al., 2019). Observations of
43 variations in groundwater level due to tidal fluctuations date back to the works of Klönne (1880),
44 Meinzer (1939), and Young (1913). However, it was only later that hydro-geomechanical models were
45 employed to elucidate these variations (Bredehoeft, 1967; Hsieh and Bredehoeft, 1987; Roeloffs, 1996;
46 Wang, 2000; Cuttillo and Bredehoeft, 2011; Kitagawa et al., 2011; Lai et al., 2013; Wang et al., 2018).
47 This progression in understanding offers a valuable opportunity to evaluate aquifer hydraulic
48 properties through the response of [groundwater to Earth tide strain fluctuations within the aquifer](#)
49 [system](#).

50 Hsieh and Bredehoeft (1987) introduced the horizontal flow model, focusing on confined conditions
51 influenced by [tidal strain within the aquifer](#). Conversely, Roeloffs (1996) and Wang (2000) explored
52 interactions within vertical flow under tidal fluctuations. Wang et al. (2018) expanded on these studies
53 by incorporating a flow from an upper aquitard, albeit assuming negligible storage within it. Later, Gao
54 et al. (2020) extended these models to include borehole skin effects. A definition of the skin effect can
55 be found in Wen et al. (2011). Thomas et al. (2023) developed an ET-GW model incorporating storage
56 and strain response in the aquitard. They applied their model to a specific site to evaluate
57 transmissivity variations and validated it using pumping tests.

58 Numerous studies have investigated aquifer hydromechanical properties by analysing GW level
59 variations induced by Earth tides, employing the models mentioned in the previous literature
60 (Narasimhan et al., 1984; Merritt, 2004; Fuentes-Arreazola et al., 2018; Zhang et al., 2019a; Shen et
61 al., 2020). [Some studies focused also on the tidal response in fractured rock aquifers \(Carr and Van Der](#)
62 [Kamp, 1969; Bower, 1983; Burbey et al., 2012; Rahi and Halihan, 2013; Sedghi and Zhan, 2016\)](#).
63 However, only a limited number of validations have been conducted, which involve comparing the
64 results with robust hydraulic assessments, such as hydraulic conductivity derived from slug testing
65 (Zhang et al., 2019b) or specific storage and transmissivity characterizations obtained through long-
66 term pumping tests (Allègre et al., 2016; Valois et al., 2022). The current evaluations predominantly
67 focus on purely confined conditions, leaving a gap in knowledge regarding tidally induced GW
68 responses in aquifers under semi-confined conditions.

69 As far as the authors are aware, the publications by Sun et al. (2020), Valois et al. (2022), and Thomas
70 et al. (2023) are the sole references addressing a comparison for a leaky aquifer. Sun et al. (2020) found
71 significant discrepancies between transmissivities obtained from Earth tide fluctuations and those

72 derived from slug or pump tests. However, it is worth noting that the comparison may be subject to
73 discussion, as the authors employed a leaky aquifer model for analysing tidally induced fluctuations,
74 whereas they used a confined aquifer model for conducting slug and pump tests. In the study
75 conducted by Valois et al. (2022), the existing Earth-Tide GroundWater (ET-GW) models, as described
76 earlier, were unable to reproduce a low semi-diurnal to diurnal amplitude ratio with positive phase
77 shifts in conjunction with pumping test transmissivity data. This discrepancy highlights the complexity
78 and challenges in modelling tidally induced groundwater responses in leaky aquifers and the need for
79 further investigation in this area.

80 We note that our previous attempts to model the observed substantial amplitude decrease from [the](#)
81 [diurnal tide \(\$O_1\$ \) to the semi-diurnal tide \(\$M_2\$ \)](#) frequency, combined with phase shifts close to zero,
82 proved unsuccessful when using Earth tide models found in the literature. None of the existing models
83 could provide satisfactory results. The pursuit of an explanation led to the realisation that analytical
84 solutions with more realistic assumptions are required. For example, aquifers are widely recognized to
85 be influenced by aquitards, which often consist of highly porous and compressible clay materials,
86 contributing significant amounts of stored water to the aquifer (Moench, 1985). Moreover, these
87 aquitards are also impacted by Earth tide strains (Bastias et al., 2022).

88 Our first objective is to develop an analytical solution considering storage and [tidal strain in the](#)
89 [aquitard](#). Unlike Thomas et al. (2023), our model incorporates borehole skin effects and allows for a
90 fixed hydraulic head at the top of the aquitard, broadening its applicability to a broader range of
91 hydrogeological conditions. The second motivation of our study is to develop a model that better fits
92 the observed results by considering aquitard storage, as evident in the pumping tests. Third, we
93 compare the results obtained from our new ET-GW model with those derived from a pumping test in
94 leaky aquifers with storage in the aquitard. Fourth, since most publications have predominantly
95 focused on assessing hydraulic properties using the semi-diurnal tide (M_2), our third motivation is to
96 demonstrate the potential of using diurnal tides (O_1) in combination with the semi-diurnal (M_2 or N_2)
97 to provide a more comprehensive characterization of aquifer and aquitard hydro-mechanical
98 properties. Our new development offers the potential to enhance hydraulic and geomechanical
99 subsurface characterization by employing a more realistic model for the groundwater response to
100 natural forces.

101

102

103 **2. Groundwater response to Earth tides in a leaky aquifer with aquitard**

104 **storage and strain**

105 Hantush (1960) pioneered the modelling of aquitard storage by modifying the leaky aquifer theory to
 106 account for storage in the aquitard. In our study, we consider a semi-confined configuration (Figure 1)
 107 where the target aquifer is overlain by an aquitard that allows for storage, strain, and vertical flux. Both
 108 layers are assumed to be slightly compressible, spatially homogenous, infinite laterally, and have
 109 constant thickness. Building upon the work of Wang et al. (2018), our research incorporates Earth Tide
 110 (ET) fluctuations into the leaky aquifer equations proposed by Moench (1985). Additionally, we
 111 incorporate the skin effect, as described by Gao et al. (2020). [2D cylindrical coordinates are used](#)
 112 [because of the radial symmetry caused by the well surrounded by hydrogeological material affected](#)
 113 [by tidal strain.](#)

114 Groundwater flow and storage in an aquifer overlain by an aquitard can be described [as \(De Marsily,](#)
 115 [1986\):](#)

$$116 \quad T \left(\frac{\partial^2 h}{\partial r^2} + \frac{1}{r} \frac{\partial h}{\partial r} \right) = S \left(\frac{\partial h}{\partial t} - \frac{BK_u}{\rho g} \frac{\partial \varepsilon}{\partial t} \right) - K' \frac{\partial h'}{\partial z} \quad (1)$$

$$117 \quad \left(\frac{\partial^2 h'}{\partial z^2} \right) = \frac{1}{D'} \left(\frac{\partial h'}{\partial t} - \frac{B'K'_u}{\rho g} \frac{\partial \varepsilon}{\partial t} \right) \quad . \quad (2)$$

118 Here, h (m) and h' (m) are the hydraulic heads in the aquifer and the aquitard respectively; h'_j (m) is
 119 the fixed hydraulic head at the top of the aquitard, r (m) is the radial distance from the studied well; T
 120 (m^2/s) and S are the aquifer transmissivity and storativity; B , B' , K_u (Pa), K'_u (Pa) are the Skempton's
 121 coefficient and the undrained bulk modulus of the aquifer and aquitard respectively; ρ (kg/m^3) and g
 122 (m/s^2) are the water density and gravity constant; ε is the volumetric Earth tide strain; K' (m/s) is the
 123 aquitard hydraulic conductivity; S'_s (m^{-1}) is the specific storage of the aquitard; D' (m^2/s) is aquitard
 124 hydraulic diffusivity (K'/S'_s ratio). Any natural regional groundwater flow is considered negligible.

125 Borehole drilling causes a zone of damage with a radius r_s (see Figure 1) that is responsible for the skin
 126 effect (Van Everdingen, 1953). A negative skin can be caused by a greater hydraulic conductivity around
 127 the well because of the material damaged by the drilling, while a positive skin can be associated by
 128 porosity clogging caused by the drilling mud. This is reflected in the well's pressure head Δh_s . The skin
 129 factor (sk) can be defined as:

$$130 \quad sk = \frac{\Delta h_s}{\left(r \frac{\partial h}{\partial r} \right)_{r=r_w}} \quad . \quad (3)$$

131 Following above assumptions, the boundary conditions are

$$132 \quad h(r, t) = h_\infty(t) \text{ at } r = \infty \quad (4)$$

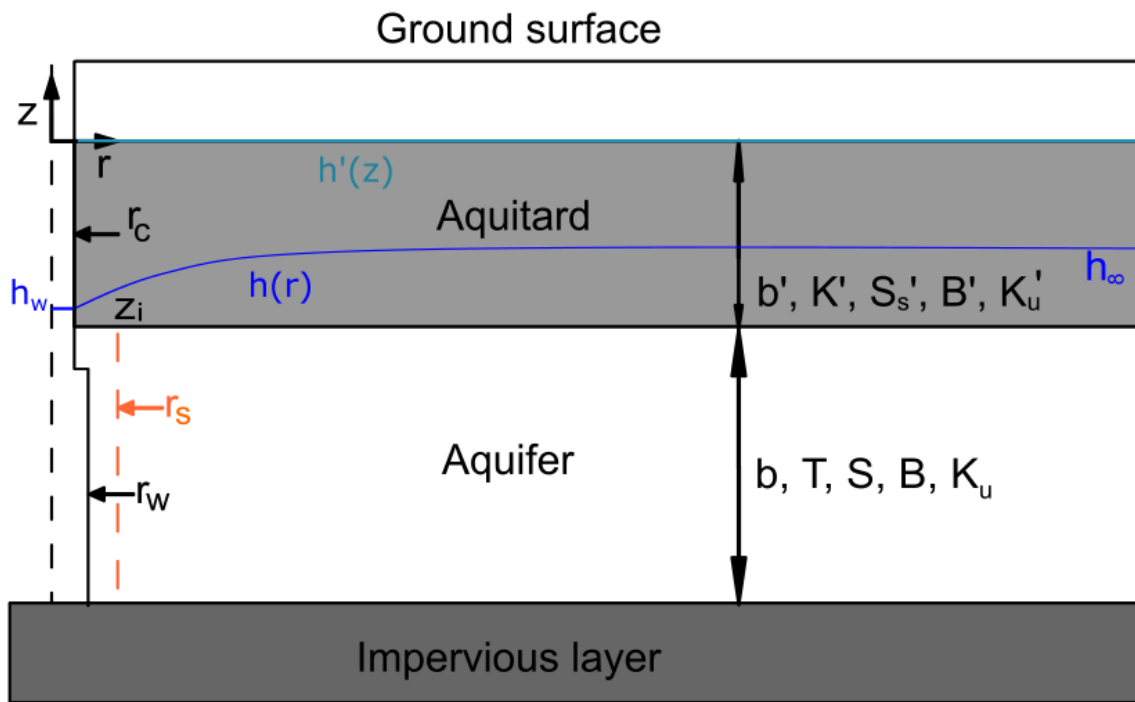
$$133 \quad h_w(t) = h(r, t) - sk \left(r \frac{\partial h(r, t)}{\partial r} \right) \text{ at } r = r_w \quad (5)$$

134
$$2\pi r_w T \left(\frac{\partial h}{\partial r} \right)_{r=r_w} = \pi r_c^2 \frac{\partial h_w}{\partial t} \quad (6)$$

135
$$h' = h \text{ at } z = z_i \quad (7)$$

136
$$h' = h'_j \text{ at } z = 0 \quad (8)$$

137 Here, t is the time (s); r_w and r_c are the radius of the well screened portion and the radius of well casing
 138 in which water level fluctuates; z_i is the aquifer-aquitard interface elevation (see Figure 1) and h_w is the
 139 hydraulic head at r_w .



140

141 *Figure 1: Semi-confined system with a compressible aquitard with storage*

142 Following Hsieh et al. (1987) and Wang et al. (2018), complex numbers were used to facilitate harmonic
 143 model development and the solution is obtained by first solving Equation 2 in the aquitard, then
 144 deriving the head response in the aquifer far away from the well (h_∞) which is independent of the
 145 radial distance. h_∞ is the aquifer response to the tidal harmonic sources far from the well. Thus, h_∞ is
 146 the aquifer hydraulic head response without any disturbance from a well-aquifer system. Then, the
 147 well effect on the aquifer response is considered by using a flux condition at the well that accounts for
 148 wellbore storage. Since h' , h , ε , h_w , h_∞ are all periodic functions, they can be expressed as:

149
$$\varepsilon(t) = \varepsilon_0 e^{i\omega t} \quad (9)$$

150
$$h_\infty(t) = h_{\infty,0} e^{i\omega t} \quad (10)$$

151
$$h_w(t) = h_{w,0}e^{i\omega t} \quad (11)$$

152
$$h(r, t) = h_0(r)e^{i\omega t} \quad (12)$$

153
$$h'(z, t) = h'_0(z)e^{i\omega t} \quad (13)$$

154 Here, $i = \sqrt{-1}$; ε_0 (m) is the ET strain amplitude and ω (s^{-1}) is the angular frequency. In this case,
 155 Equation 2 becomes:

156
$$\left(\frac{\partial^2 h'_0}{\partial z^2}\right) = \frac{1}{D'} \left(i\omega h'_0 - i\omega \frac{B'K'_u}{\rho g} \varepsilon_0 \right) \quad (14)$$

157 According to Wang (2000) and Roeloffs (1996) and as detailed in appendix A, the solution of Equation
 158 2 is:

159
$$h'_0 = A_1 e^{\frac{(1+i)}{\delta}(z-z_i)} + A_2 e^{-\frac{(1+i)}{\delta}(z-z_i)} + \frac{B'K'_u}{\rho g} \varepsilon_0 \quad (15)$$

160 where $\delta = \left(\frac{2D'}{\omega}\right)^{1/2}$. Thus, at the interface between the aquifer and the aquitard ($z=z_i$), we have
 161 pressure continuity as $h'(z_i, t) = h_0 e^{i\omega t} = h(t)$ which leads to:

162
$$\left(\frac{\partial h'}{\partial z}\right)_{z=z_i} = \frac{1+i}{\delta} \left(\frac{h_0 - \frac{B'K'_u}{\rho g} \varepsilon_0}{\tanh\left(\frac{1+i}{\delta} z_i\right)} - \frac{h'_j - \frac{B'K'_u}{\rho g} \varepsilon_0}{\sinh\left(\frac{1+i}{\delta} z_i\right)} \right) e^{i\omega t} \quad (16)$$

163 Equation 16 is in agreement with Butler and Tsou (2003) where leakage is shown to be a scale-invariant
 164 phenomenon.

165 Equation 1 can be solved far away from the well using h_∞ which is independent of the radial distance
 166 from the well and by using the source term from h' as follows

167
$$0 = \frac{\partial h_\infty}{\partial t} - \frac{BK_u}{\rho g} \frac{\partial \varepsilon}{\partial t} - \frac{K'}{S} \frac{1+i}{\delta} \left(\frac{h_\infty - \frac{B'K'_u}{\rho g} \varepsilon_0}{\tanh\left(\frac{1+i}{\delta} z_i\right)} - \frac{h'_j - \frac{B'K'_u}{\rho g} \varepsilon_0}{\sinh\left(\frac{1+i}{\delta} z_i\right)} \right) e^{i\omega t} \quad (17)$$

168
$$h_{\infty,0} = \frac{BK_u}{\rho g} \varepsilon_0 \frac{Si\omega + K' \frac{1+i}{\delta} \frac{B'K'_u}{BK_u} \left(\frac{-1}{\tanh\left(\frac{1+i}{\delta} z_i\right)} - \frac{h'_j - \frac{B'K'_u}{\rho g} \varepsilon_0}{\sinh\left(\frac{1+i}{\delta} z_i\right)} \right)}{Si\omega - K' \frac{1+i}{\delta} \frac{1}{\tanh\left(\frac{1+i}{\delta} z_i\right)}} \quad (18)$$

169 The disturbance in water level due to the well can be expressed as:

170
$$s(r, t) = h(r, t) - h_\infty(t) \quad (19)$$

171 By expressing Equation 1 with the sum of s and h_∞ (Eq. 19), and using Equation 16 to express the leaky
 172 component and using equation 17 to remove h_∞ , it follows:

173
$$T \left(\frac{\partial^2 s}{\partial r^2} + \frac{1}{r} \frac{\partial s}{\partial r} \right) = S \left(\frac{\partial s}{\partial t} \right) - K' \frac{1+i}{\delta} s \frac{1}{\tanh \left(\frac{1+i}{\delta} z_i \right)} \quad (20)$$

174 with the boundary conditions:

175
$$s(r \rightarrow \infty) = 0 \quad (21)$$

176
$$h_{w,0} - h_{\infty,0} = s - sk \left(r \frac{\partial s}{\partial r} \right) \quad \text{at } r = r_w \quad (22)$$

177
$$2\pi r_w T \left(\frac{\partial s}{\partial r} \right)_{r=r_w} = i\omega \pi r_c^2 h_{w,0} \quad (23)$$

178 The solution of this differential equation is $s(r) = C_I I_0(\beta r) + C_K K_0(\beta r)$ (Wang *et al.*, 2018), where I_0
 179 and K_0 are the modified Bessel functions of the first and second kind and the zeroth order, respectively.

180 Further,

181
$$\beta = \left(\frac{i\omega S}{T} - \frac{K' (1+i)}{T \delta} \frac{1}{\tanh \left(\frac{1+i}{\delta} z_i \right)} \right)^{1/2} \quad (24)$$

182 The boundary conditions lead to $C_I=0$ and $C_K = -\frac{i\omega r_c^2 h_{w,0}}{2T\beta r_w K_1(\beta r_w)}$ because $\frac{dK_0(r)}{dr} = -K_1(r)$. Therefore,
 183 the final solution for the well water level is:

184
$$h_{w,0} = \frac{BK_u}{\rho g} \varepsilon_0 \frac{Si\omega + K' \frac{1+i}{\delta} \frac{B' K'_u}{BK_u} \left(\frac{-1}{\tanh \left(\frac{1+i}{\delta} z_i \right)} - \frac{h'_j \frac{\rho g}{B' K'_u \varepsilon_0} - 1}{\sinh \left(\frac{1+i}{\delta} z_i \right)} \right)}{\sigma \left(Si\omega - K' \frac{1+i}{\delta} \frac{1}{\tanh \left(\frac{1+i}{\delta} z_i \right)} \right)} \quad (25)$$

185 where

186
$$\sigma = 1 + \frac{i\omega r_c^2 K_0(\beta r_w)}{2T\beta r_w K_1(\beta r_w)} + \frac{i\omega r_c^2}{2T} sk \quad (26)$$

187 By assuming $h'_j = 0$ (i.e. the hydraulic head at the top of the aquitard corresponds to the
 188 unsaturated-saturated interface at $z=0$), Equation 25 can be reorganized to

189
$$h_{w,0} = \frac{BK_u}{\rho g} \varepsilon_0 \frac{Si\omega + K' \frac{1+i}{\delta} R_{KuB} \left(\frac{1 - \cosh \left(\frac{1+i}{\delta} z_i \right)}{\sinh \left(\frac{1+i}{\delta} z_i \right)} \right)}{\sigma \left(Si\omega - K' \frac{1+i}{\delta} \frac{1}{\tanh \left(\frac{1+i}{\delta} z_i \right)} \right)} \quad (27)$$

190 where

191
$$R_{KuB} = \frac{K'_u B'}{K_u B} \quad (28)$$

192 By disregarding $\frac{BK_u}{\rho g}$ product which only controls the amplitude, the solution has six independent
193 parameters which are T, S, K', D', sk and the R_{KuB} ratio.

194 Let us now define the amplitude response (or amplitude ratio), A , and phase shift, α , of the GW
195 response to ET fluctuations:

$$196 \quad A = \left| h_{w,0} / \frac{BK_u}{\rho g} \varepsilon_0 \right| \quad (29)$$

$$197 \quad \alpha = \arg \left[h_{w,0} / \frac{BK_u}{\rho g} \varepsilon_0 \right]. \quad (30)$$

198 Figure 2 shows the amplitude response and phase shift as a function of frequency using our new
199 solution in comparison to key models reported in the literature. Aquitard parameters were set accoring
200 to Batlle-Aguilar et al. (2016), while aquifer parameters were chosen accoring to the field application
201 below. We validate the solution using a very low aquitard conductivity (10^{-14} m/s), so that we can
202 compare it to the horizontal flux with wellbore storage model (Hsieh et al., 1987). It shows a perfect
203 match.

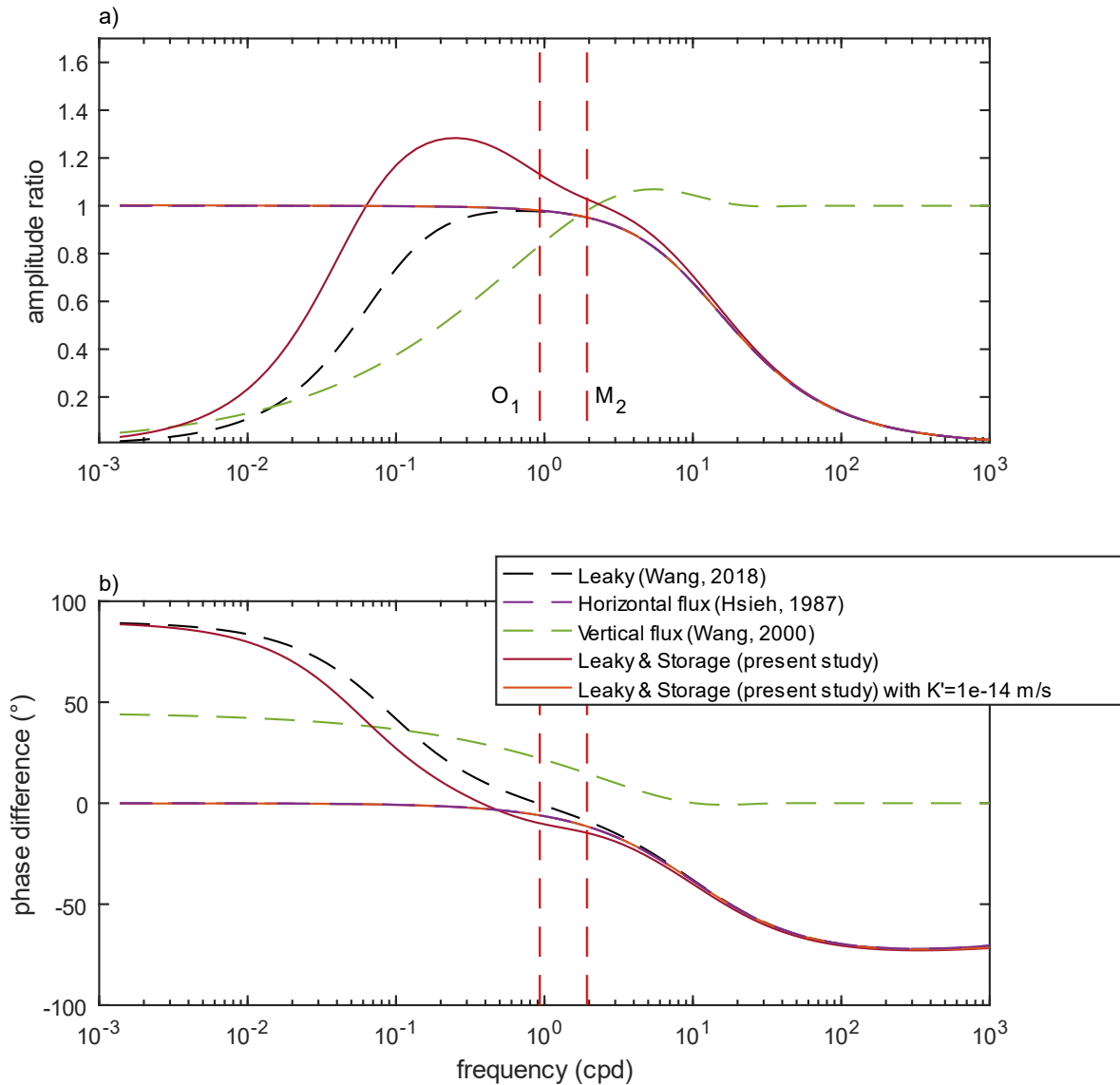
204 Because both horizontal and vertical flux models are associated with opposite phase shift signs (Figure
205 2b), the latter can offer valuable insights for model selection (Allègre et al., 2014). Positive phase shifts
206 in the vertical flux model are related to an increasing amplitude ratio with frequency, whereas the
207 wellbore storage model exhibits the opposite behaviour. Wang et al. (2018) developed a leaky model
208 capable of demonstrating both positive and negative phase shifts, where positive phase shifts
209 correspond to an increasing amplitude ratio with frequencies, and negative phase shifts are linked to
210 a decreasing amplitude ratio.

211 Our new model showcases positive or negative phase shifts with an increasing or decreasing amplitude
212 ratio over frequency, even allowing for amplitude ratios greater than one. Notably, Wang (2000)
213 observed a similar characteristic in the vertical flux model, with an amplitude just above one (1.06) for
214 very specific conditions. At high frequencies, our model displays amplitude ratios and phase shifts
215 similar to those of the leaky and wellbore storage models, reflecting the attenuation of high-frequency
216 pore pressure fluctuations in the aquifer by well water.

217 At low frequencies (Fig. 2), the purely confined model exhibits a constant phase shift (0°) and
218 amplitude ratio (1). This constant behavior is the signature of the absence of well impact on
219 groundwater level fluctuations and the absence of phase shift between the Earth tide strain and the
220 aquifer level fluctuations. It means that the groundwater fluctuations of the aquifer are the same as
221 the groundwater fluctuations in the well (absence of amplification/attenuation and phase shifts) and
222 that there is no phase shift between the strain and the water pressure variations inside the aquifer.

223 For the "Leaky & Storage (present study)" model (Fig. 2), the leaky conditions do provoke a phase shift
 224 and an amplitude modification as compared to purely confined. Such values of phase shift and
 225 amplitude modification do vary with frequency.

226



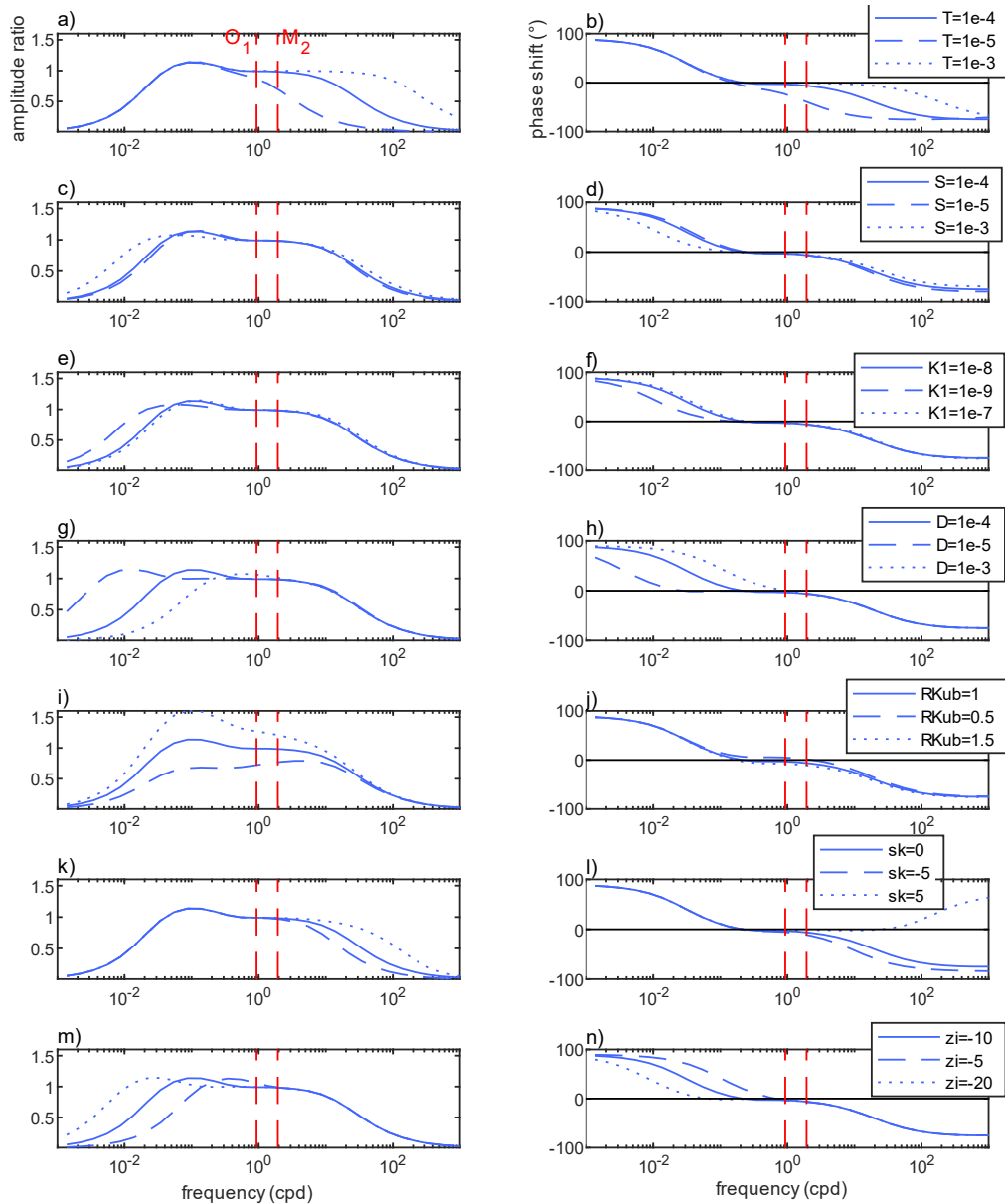
227

228 *Figure 2: Frequency variation of amplitude response and phase shift of the groundwater response to Earth tides. The*
 229 *transmissivity (T) is $10^{-5} \text{ m}^2/\text{s}$, storativity (S) is 10^{-4} , hydraulic conductivity of the aquitard (K') is 10^{-8} m/s , aquitard hydraulic*
 230 *diffusivity (D') is $10^{-4} \text{ m}^2/\text{s}$, skin factor (sk) is 0, R_{KuB} to 1.4, well casing radius (r_c) and screen radius (r_w) is 6.03 cm. b' was set*
 231 *to 5 m. Screen depth (z) was set to 23 m for the vertical flow model of Wang (2000).*

232

233 We explored the parameter space by focussing on the frequency-dependant amplitude response and
 234 phase shift responses for different sets of parameter values. The reference parameter set is the one

235 described above. T , R_{KUB} and z_i have a large impact on model shapes. As also observed by Hsieh et al.
 236 (1987), S does not have a major impact on the results (Fig3c and 3d). The skin effect does not play a
 237 large role in the useful frequency band (about 1 to 2 cpd) for amplitudes, but its influence is larger for
 238 the phase shifts when compared to the reference parameter set. K' does not significantly influence the
 239 results with respect to the reference parameter set used in the study (Figures 3e to 3f). K' has the
 240 opposite role of S and they appear to compensate each others effects, because of their respective role
 241 in Equation 27.

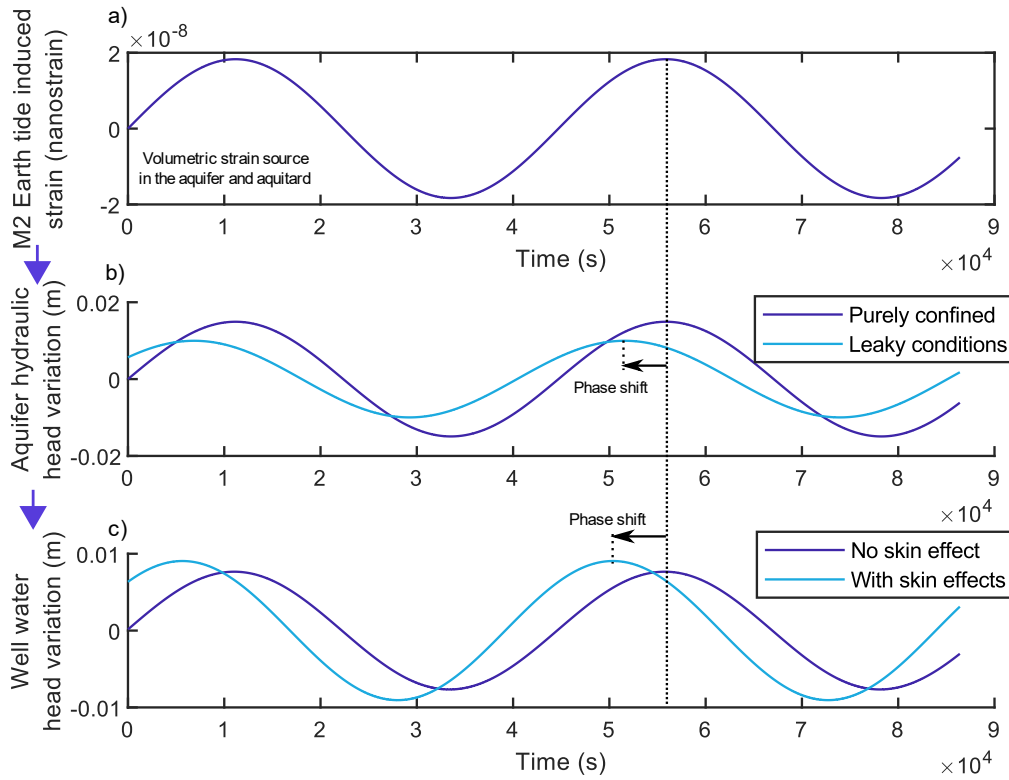


242

243 *Figure 3: Illustration of the amplitude response (left column) and phase shift (right column) as a function of frequency for*
 244 *various parameters compared to the reference parameter set.*

245 Figure 4 shows the impacts of considering leaky and skin effects for a realistic parameter set. Purely
 246 confined conditions (no leaky aquitard) do not create a phase shift between the volumetric strain in

247 the aquifer (Fig 4a) and the associated hydraulic head variation (Fig 4b), while a compressible and leaky
 248 aquitard (Fig 4b) or skin effects around the well (Fig 4c) could involve positive phase shifts.



249
 250 *Figure 4: Example of the volumetric strain time series generated by the M2 Earth tide in a), which creates aquifer hydraulic*
 251 *head variations in b), resulting in well water level variations in c). The transmissivity (T) is $10^{-6} \text{ m}^2/\text{s}$, storativity (S) is $7 \cdot 10^{-4}$,*
 252 *hydraulic conductivity of the aquitard (K') is 10^{-6} m/s , aquitard hydraulic diffusivity (D') is $10^{-4} \text{ m}^2/\text{s}$, skin factor (sk) is -5 m, z_1*
 253 *to -10 m, RKuB to 0.3, well casing radius (r_c) and screen radius (r_w) is 6.03 cm. B is set to 0.8 and K_u to 10 GPa.*

254

255

256

257 **3. Application of the new model to a groundwater monitoring dataset from Cambodia**

258 **3.1 Field site and previous results**

259 The field site in Northwest Cambodia comprises three boreholes drilled into the subsurface, consisting
260 of mudstone, claystone, siltstone, and sandstone. Time series and pumping test results have been
261 reported in Valois et al. (2022), while details of the lithology can be found in Vouillamoz et al. (2012;
262 2016) and Valois et al. (2017; 2018; 2022). Pumping from the aquifer is limited by a very low specific
263 yield, attributed to the presence of fine deposits such as clay and mudstone (Vouillamoz et al. 2012;
264 Valois et al., 2018).

265 The boreholes were drilled to a depth of 31 meters with a radius of 6 inches and equipped with 4-inch
266 PVC casing from top to bottom, featuring a 9-meter long screen at the hole's base. The aquifer is
267 situated within a hard rock media, comprising either claystone or sandstone, located beneath a 10-
268 meter thick clay layer.

269 For the pumping tests, the wells were pumped for three days, and water levels were allowed to recover
270 for four days in two observation wells. The interpretation of the pumping tests utilized
271 AQTESOLV™/Pro v4.5 software, employing the leaky aquifer with aquitard storage model (Moench,
272 1985) or a 3D flow using the generalized radial flow model (Barker, 1988). The selected solutions,
273 compared to other models (Theiss, Hantush without aquitard storage), demonstrated the best fit with
274 a Root Mean Square Error (RMSE) of 0.02 m for Cambodia.

275

276 **3.2 Well sensitivities and phase shifts to Earth tides**

277 Between 2010 and 2015, well water levels were measured at 20, 40, or 60-minute intervals using
278 absolute pressure sensors (Diver data loggers, Eijkelkamp Soil & Water, NL). To compensate for
279 barometric pressure (BP) effects, data from a barometer located a few kilometres away from the field
280 site were utilized (Eijkelkamp Soil & Water, NL). A zero-phase Butterworth filter was employed to
281 eliminate low-frequency content (periods longer than 10 days) from both groundwater (GW) and BP
282 data.

283 For each site's geolocation (latitude, longitude, and height), ET strain time series were computed at
284 20-minute intervals using SPOTL software (Agnew, 2012). The time series were then modelled using
285 Harmonic Least-Squares (HALS; Schweizer et al., 2021) with eight frequencies corresponding to the
286 major tides (Table 1) following Merritt's description (2004). HALS provides amplitude and phase
287 estimations for each tidal component and record.

288

289
290

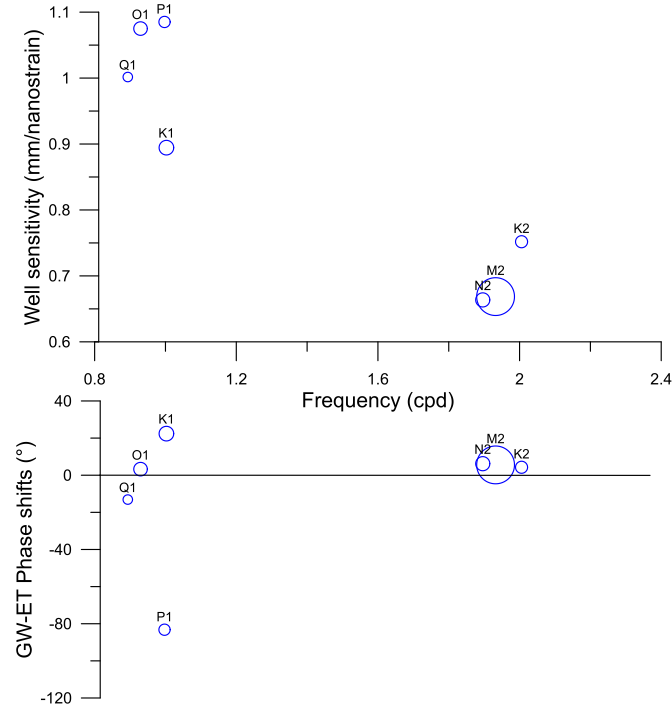
Table 1. Dominant tidal components that are generally found in groundwater measurements
(adapted from MacMillan et al., 2019)

Darwin Name	Frequency (cpd)	Attribution
Q_1	0.89365	Earth
O_1	0.929536	Earth
P_1 -	0.997262	Earth
S_1	1.000000	Atmosphere
K_1	1.002738	Earth
N_2	1.895982	Earth
M_2	1.932274	Earth
S_2	2.000000	Earth/Atmosphere
K_2	2.005476	Earth

291

292 The results obtained from HALS were utilized to calculate the amplitude response and phase shift
293 between groundwater (GW) and Earth tide (ET) for each tidal component. These amplitude responses
294 are commonly known as "well sensitivities" to Earth tide strains (Rojstaczer and Agnew, 1989) and are
295 summarized in Figure 5 alongside the corresponding phase shifts.

296 The well sensitivities to tides exhibit a frequency-dependent behaviour, resulting in similar values for
297 neighbouring frequencies and a generally decreasing magnitude. The amplitudes of M_2 and N_2 are
298 relatively straightforward to assess due to their significant magnitudes (11.2 and 2.1 mm, respectively),
299 and their amplitude responses and phase shifts are highly similar. The phase shifts for the tides of
300 interest (O_1 , N_2 , and M_2) are positive. However, the signs of the amplitudes for the other tides can be
301 attributed to their low amplitude responses, which are challenging to characterize using HALS.



302

303 *Figure 5: Amplitude responses and phase shifts as a function of frequency for the Cambodian site. S1 and S2 were excluded*
 304 *as they are not only generated by Earth tides. The circle size is proportional to the amplitude in the well water levels.*

305

306 3.3 Fitting the M_2/O_1 amplitude response ratio and phase shifts

307 The analysis is restricted to two types of tides: the semi-diurnal and diurnal tides. This limitation arises
 308 because the magnitude of Earth tide-induced well water levels is significantly damped for higher
 309 frequencies, making it difficult to discern and analyse tides beyond these two types. Here, we use
 310 amplitude responses (A_{M_2}, A_{O_1}) and phase shifts ($\alpha_{M_2}, \alpha_{O_1}$) to estimate hydraulic subsurface properties.
 311 N_2 tide was not used since its response may be too similar to M_2 and does not help with constraining
 312 the model. Amplitudes are influenced by geomechanical parameters (BK_u) which are generally not
 313 considered in classical hydrogeology. Valois et al. (2022) previously illustrated that the M_2 to O_1
 314 amplitude response ratio can be computed because it is not directly multiplied by BK_u and because it
 315 provides useful information about model choice. This leads to a system of three equations and six
 316 parameters ($T, S, K', D', skin$, and R_{KuB}) by using the simplified model in Equation 27 when the geometry
 317 of the well and the aquitard-aquifer system is known:

318
$$\frac{A_{M_2}}{A_{O_1}} = \left| h_{w,0,\omega=M_2} / h_{w,0,\omega=O_1} \right| \quad (31)$$

319
$$\alpha_{M_2} = \arg \left[h_{w,0,\omega=M_2} / \frac{BK_u}{\rho g} \varepsilon_0 \right] \quad (32)$$

320
$$\alpha_{O_1} = \arg \left[h_{w,0,\omega=O_1} / \frac{BK_u}{\rho g} \varepsilon_0 \right]. \quad (33)$$

321 Table 2 displays the data to be fitted using the three equations above.

322 Table 2: Data to be fitted using the ET-GW model

	$\frac{A_{M2}}{A_{O1}}$	α_{M2} (°)	α_{O1} (°)
Cambodia	0.62	5.62	3.3

323

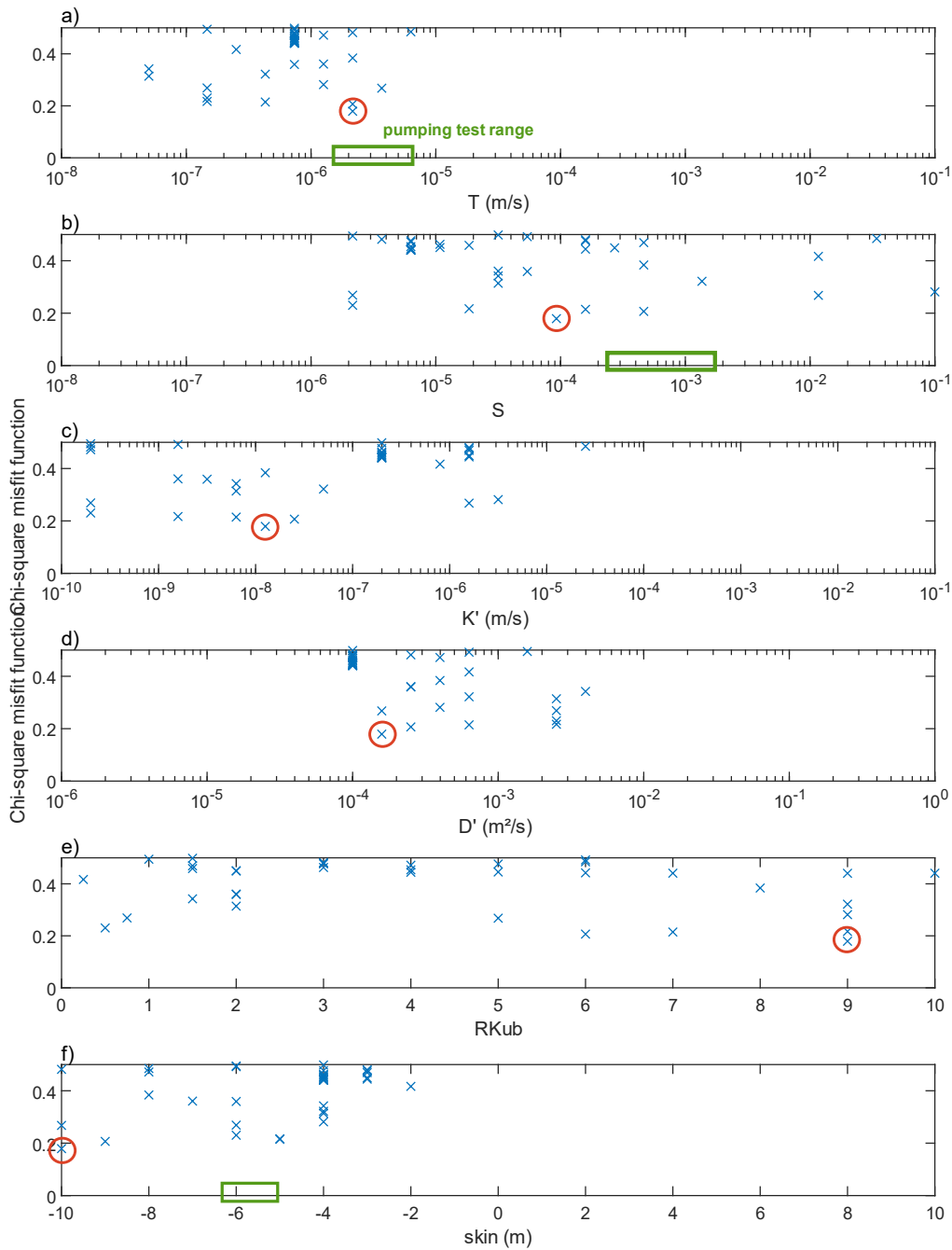
324 A systematic exploration of the entire parameter space without any constraints other than the well
 325 and aquifer geometry was carried out. Hydraulic and geomechanical property ranges are chosen
 326 according to the literature, i.e., De Marsily (1986) and Domenico and Schwartz (1998). In order to
 327 assess the goodness of fit with the three observed parameters (Eqs 31 to 33), the objective chi-square
 328 function is defined below:

329
$$\chi^2 = 1/N \sum_{i=1}^N \left(\frac{(Obs_i - Mod_i)}{Error_i} \right)^2 \quad (34)$$

330 where N is the number of observed parameters (3 here), Obs_i , Mod_i and $Error_i$ are the observed
 331 parameter, modeled parameter and their errors respectively. Thus, this objective function takes into
 332 account errors of the observed parameters (De Pasquale et al.; 2022). They were set to 0.1°, 0.5° and
 333 0.2 for α_{M2} , α_{O1} and $\frac{A_{M2}}{A_{O1}}$ respectively, according to Valois et al. (2022).

334

335 The model allows to fit both O_1 and M_2 positive phases and the low M_2 to O_1 amplitude ratio (misfit
 336 closed to 0 in Fig. 6), whereas the model of Gao et al (2020) cannot (misfit above 1 see Appendix B,
 337 and Valois et al., 2020). The T value is in good agreement with the pumping test range (Fig. 6a). S is
 338 half an order of magnitude below the pumping test range (Fig 6b) whereas the storativity best-fit for
 339 Gao et al (2020) is two orders of magnitude above (Appendix B). The skin effect also shows acceptable
 340 values as compared to the pumping test (Fig 6f). The parameter exploration shows best-fits for K' and
 341 D' , whereas it is difficult to identify a clear best-fit for the R_{KuB} parameter. The values are within the
 342 expected range for the hydrogeological configuration: The mudstone aquitard has a lower hydraulic
 343 conductivity (10^{-8} m/s) than the underlying claystone aquifer (coarser grain size than the aquitard, with
 344 a K value of about 10^{-7} m/s for an aquifer thickness of 22 m), and a diffusivity of about 10^{-4} m²/s. This
 345 is in agreement with the aquitard classification of Pacheco (2013).



346

347 *Figure 6: Results of full parameters exploration using the leaky with storage aquifer model for the Cambodian case study. Red*
 348 *circles represent the best-fit.*

349

350 4. DISCUSSION

351 4.1. Uncertainties and discrepancies

352 There are several sources of uncertainty which originate from measurement and their propagation as
 353 well as uncertainties introduced by model assumptions. We believe that uncertainties linked to

354 pressure sensor resolution (0.2 mm) and time resolution (20 minutes) as well as the HALS
355 decomposition were too low to be worth considering, at least for the semi-diurnal tides. This can be
356 deduced from the nearly identical amplitude responses at M_2 and N_2 at our field site. Because those
357 responses are indeed identical, it means that errors in the raw data set did not influence the response
358 characterization. We note that amplitude responses and phase shifts show larger discrepancies for the
359 diurnal tides. This could be linked to overall lower amplitudes which are generally more difficult to
360 characterise. We therefore conclude that errors arising from uncertainties are negligible compared to
361 the uncertainty introduced by model assumptions, in agreement with Sun *et al.* (2020).

362 Discrepancies between hydro-geomechanical properties derived from the groundwater response to
363 Earth tides (termed as “passive” and assuming a compressible matrix) and hydraulic testing (e.g., slug,
364 pump and lab testing, termed as “active” and generally assuming an incompressible matrix) have been
365 reported in the literature and have not been appropriately reconciled. By fitting amplitude response
366 ratio and phase shifts (Section 3.3), a T value discrepancy of one order of magnitude can be observed
367 between both approaches. We hypothesise that this is caused by parameter anisotropy.

368 Zhang *et al.* (2019b) pointed out differences in hydraulic conductivities of more than one order of
369 magnitude between ET analysis and slug tests and attributed this to differences in the investigated
370 scale. Allègre *et al.* (2016) reported much higher values of storativity derived from pumping test is
371 compared to ET when using the vertical flow model. Sun *et al.* (2020) showed that T values are
372 frequency-dependent with several orders of magnitude differences when comparing co-seismic, ET,
373 slug or pump test methods. The discrepancies can be explained by the different conceptual models
374 used in the active (based on perfectly confined) and passive methods (based on leaky conditions) or
375 by the frequency dependency of hydraulic parameters. The literature illustrates that transmissivity,
376 hydraulic conductivity or specific storage can indeed vary depending on the frequency of the forcing
377 (e.g., Cartwright *et al.*, 2005; Renner and Messar, 2006; Guiltinan and Becker, 2015; Rabinovich *et al.*,
378 2015). This demonstrates the need for attention when assessing hydraulic parameters using passive
379 methods for semi-confined conditions. We specifically emphasise the need for using the same
380 conceptual model (i.e., confined, leaky with or without storage, vertical flow) when comparing active
381 and passive methods, as well as the need of preliminary hydrogeological knowledge of both the aquifer
382 system (i.e., presence of an aquitard with or without storage) (Bastias *et al.*, 2022) as well as the
383 borehole skin effect.

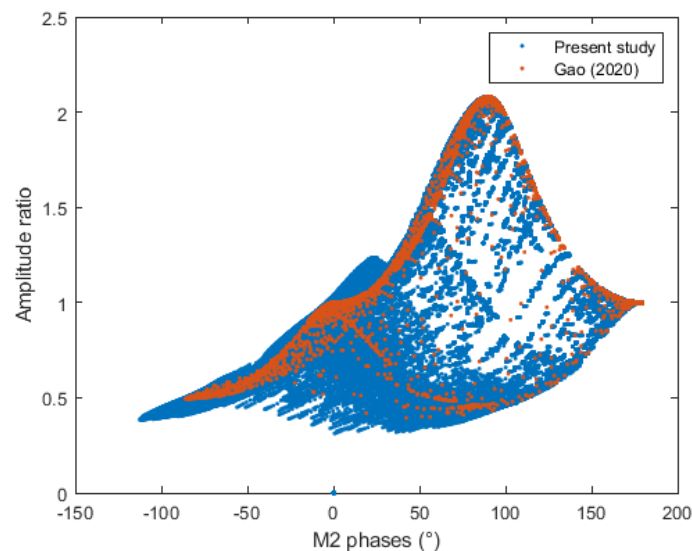
384

385 **4.2. The use of the leaky model with aquitard storage**

386 Our new analytical solution describing the well water level response to harmonic Earth tide strains
387 contains at least six hydro-geomechanical parameters that could be derived from only three features,

388 e.g., M_2 to O_1 amplitude response ratio and M_2 and O_1 phase shifts. Applying this model to real-world
389 cases to derive properties from amplitude responses and phase shifts provides relevant information
390 on T , S , D' , K' , and skin effect, but it is prone to non-uniqueness. Thus, a priori information may be
391 needed depending on the capacity of the inverse problem to fit observed data (phases shifts and
392 amplitude ratio). In our case study, parameter assessment would benefit from prior information on S
393 (or K') and R_{KuB} .

394 The model presented in this study can be useful when the hydrogeological configuration involves
395 storage in the aquitard with fixed head (i.e., Dirichlet) boundary conditions and for cases where phase
396 shifts and amplitude ratio do exemplify a specific pattern. For example, when compared to Gao et al
397 (2020) and using the parametrization of the present study (Fig. 7), our solution is able to model lower
398 M_2 to O_1 amplitude ratio, lower phases, and higher amplitude ratio for phases closed to 0.



399

400 *Figure 7: Outputs of the models using the parametrization of the study ($rc=rw=6.08$ cm, $z_i=-10$ m).*

401

401 While the amplitudes are controlled by the product of the Skempton coefficient and the undrained
402 bulk modulus, these mechanical parameters also affect phase shifts. Therefore, further investigations
403 are needed to assess these influences using other methods or to link them empirically with the
404 hydraulic parameters. This is crucial to enhance confidence in utilizing groundwater response to Earth
405 tides as a valuable tool for better understanding and characterizing groundwater resources.

406

407 **5. Conclusion**

408 We have developed a new analytical solution for the well water level response to Earth tide strains.
409 This solution considers a previously unprecedented physical reality, specifically, a leaky aquifer with
410 aquitard storage, subject to Dirichlet boundary conditions under tidal strain. Additionally, our model
411 considers the influence of borehole storage and skin effects, further improving the accuracy and
412 comprehensiveness of the analysis. This model extends upon previous models and allows advanced
413 characterization of the subsurface using the groundwater response to natural forces. The new model
414 overcomes previous limitations, for example it explains very low M_2 to O_1 amplitude ratios as well as
415 large phase shift difference between M_2 and O_1 tides. The model relies on six combinations of hydro-
416 geomechanical parameters. In this study, we assess the most sensitive parameters to be the
417 transmissivity, the well skin effect, the aquitard to aquifer mechanical parameters ratio ($B'K_u'/BK_u$), as
418 well as aquitard diffusivity and aquitard conductivity to aquifer storativity ratio.
419 We apply our new model to a groundwater monitoring dataset from Cambodia and compare the
420 results with pumping tests undertaken in the same formation. We used the diurnal (O_1) and semi-
421 diurnal (M_2) tides to better constrain the model. Results illustrate significant insight into subsurface
422 properties. For example, we derive relevant information about T , S , D' , K' , and *skin effect*, when
423 compared to the pumping test results. Overall, our new model can be used to shed light on previously
424 inexplicable well water level behaviour and can be paired with other investigation methods to enhance
425 understanding of subsurface processes.

426

427 **Competing interests**

428 The contact author has declared that none of the authors has any competing interests.

429 **Acknowledgements**

430 This work has been carried out in the framework of the Institut de Recherche pour le Développement
431 and the French Red Cross collaborative project 39842A1 - 1R012-RHYD, with the financial support of
432 the European Community (grant DIPECHO SEA ECHO/DIP/BUD/2010/01017 and grant DCI-
433 FOOD/2011/278-175).

434 **Code/Data availability**

435 The authors thank the Github platform for hosting the field data in
436 <https://github.com/remival/CambodiaData-for-leaky-and-compressible-aquiatrd.git>

437

438 **Author contribution**

439 RV did the field survey, analysis and coordinate the paper writing. AR verified model theory and
440 participated to the writing. JMV did the field and participated to the writing. GCR participated to the
441 data analysis and paper writing.

442

443 **References**

- 444 Agnew, D. C. (2012), SPOTL: Some programs for ocean-tide loading, SIO technical report, Scripps
445 Institution of Oceanography, UC San Diego, Calif. [Available at
446 http://escholarship.org/uc/sio_techreport.]
- 447 Allègre, V., Brodsky, E. E., Xue, L., Nale, S. M., Parker, B. L., & Cherry, J. A. (2016). Using earth-tide
448 induced water pressure changes to measure in situ permeability: A comparison with long-term
449 pumping tests. *Water Resources Research*, 52(4), 3113-3126.
- 450 Barker, J. A. (1988). A generalized radial flow model for hydraulic tests in fractured rock. *Water*
451 *Resources Research*, 24(10), 1796-1804.
- 452 Bastias Espejo, J. M., Rau, G. C., & Blum, P. (2022). Groundwater responses to Earth tides: Evaluation
453 of analytical solutions using numerical simulation. *Journal of Geophysical Research: Solid Earth*,
454 127, e2022JB024771. <https://doi.org/10.1029/2022JB024771>
- 455 Batlle-Aguilar, J., Cook, P.G., Harrington, G.A., 2016. Comparison of hydraulic and chemical methods
456 for determining hydraulic conductivity and leakage rates in argillaceous aquitards. *J. Hydrol.* 532,
457 102–121. <https://doi.org/10.1016/j.jhydrol.2015.11.035>
- 458 Bower, D. R. (1983). Bedrock fracture parameters from the interpretation of well tides. *Journal of*
459 *Geophysical Research: Solid Earth*, 88(B6), 5025-5035.
- 460 Burbey, T. J., Hisz, D., Murdoch, L. C., & Zhang, M. (2012). Quantifying fractured crystalline-rock
461 properties using well tests, earth tides and barometric effects. *Journal of Hydrology*, 414, 317-328.
- 462 Butler Jr, J. J., & Tsou, M. S. (2003). Pumping-induced leakage in a bounded aquifer: An example of a
463 scale-invariant phenomenon. *Water resources research*, 39(12).
- 464 Bredehoeft, J. D. (1967). Response of well-aquifer systems to earth tides. *Journal of Geophysical*
465 *Research*, 72(12), 3075-3087.
- 466 Carr, P. A., & Van Der Kamp, G. S. (1969). Determining aquifer characteristics by the tidal method.
467 *Water Resources Research*, 5(5), 1023-1031.
- 468 De Marsily G (1986) *Quantitative hydrogeology*. Academic, San Diego, CA.
- 469 De Pasquale, G., Valois, R., Schaffer, N., & MacDonell, S. (2022). Contrasting geophysical signatures of
470 a relict and an intact Andean rock glacier. *The Cryosphere*, 16(5), 1579-1596.

471 Domenico PA, Schwartz FW (1998) Physical and chemical hydrogeology, 2nd edn. Wiley, Chichester,
472 UK.

473 Cartwright, N., Nielsen, P., & Perrochet, P. (2005). Influence of capillarity on a simple harmonic
474 oscillating water table: Sand column experiments and modeling. *Water resources*
475 *research*, 41(8).Cutillo, P. A., & Bredehoeft, J. D. (2011). Estimating aquifer properties from the
476 water level response to Earth tides. *Groundwater*, 49(4), 600-610.

477 Fuentes-Arreazola, M. A., Ramírez-Hernández, J., & Vázquez-González, R. (2018). Hydrogeological
478 properties estimation from groundwater level natural fluctuations analysis as a low-cost tool for
479 the Mexicali Valley Aquifer. *Water*, 10(5), 586.

480 Gao, X., Sato, K., & Horne, R. N. (2020). General Solution for Tidal Behavior in Confined and
481 Semiconfined Aquifers Considering Skin and Wellbore Storage Effects. *Water Resources Research*,
482 56(6), e2020WR027195.

483 Gultinan, E., & Becker, M. W. (2015). Measuring well hydraulic connectivity in fractured bedrock using
484 periodic slug tests. *Journal of Hydrology*, 521, 100-107.

485 Hantush, M. S. (1960). Modification of the theory of leaky aquifers. *Journal of Geophysical Research*,
486 65(11), 3713-3725.

487 Hsieh, P. A., Bredehoeft, J. D., & Farr, J. M. (1987). Determination of aquifer transmissivity from Earth
488 tide analysis. *Water resources research*, 23(10), 1824-1832.

489 Kitagawa, Y., Itaba, S., Matsumoto, N., & Koizumi, N. (2011). Frequency characteristics of the response
490 of water pressure in a closed well to volumetric strain in the high-frequency domain. *Journal of*
491 *Geophysical Research: Solid Earth*, 116(B8).<https://doi.org/10.1029/2010JB007794>

492 Klönne, F. W. (1880). Die periodischschwankungen des wasserspiegels in den
493 inundiertenkohlschachten von Dux in der period von 8 April bis 15 September 1879 (The periodic
494 fluctuations of water levels in the flooded coal mine at Dux in the period 8 April to 15 September
495 1879). *Sitzungsberichte Kaiserliche Akademie der Wissenschaften in Wien*.

496 Kuang, X., Jiao, J. J., Zheng, C., Cherry, J. A., & Li, H. (2020). A review of specific storage in aquifers.
497 *Journal of Hydrology*, 581, 124383.

498 Lai, G., Ge, H., & Wang, W. (2013). Transfer functions of the well-aquifer systems response to
499 atmospheric loading and Earth tide from low to high-frequency band. *Journal of Geophysical*
500 *Research: Solid Earth*, 118(5), 1904-1924.

501 McMillan, T. C., Rau, G. C., Timms, W. A., & Andersen, M. S. (2019). Utilizing the impact of Earth and
502 atmospheric tides on groundwater systems: A review reveals the future potential. *Reviews of*
503 *Geophysics*, 57(2), 281-315.

504 Meinzer, O. E. (1939). Ground water in the United States, a summary of ground-water conditions and
505 resources, utilization of water from wells and springs, methods of scientific investigation, and

506 literature relating to the subject, (Tech. Rep. 1938-39). U.S. Department of the Interior, Geological
507 Survey. <https://doi.org/10.3133/wsp836D>

508 Melchior, P. (1983). *The tides of the planet Earth*. Oxford.

509 Merritt, M. L. (2004). *Estimating hydraulic properties of the Floridan aquifer system by analysis of*
510 *earth-tide, ocean-tide, and barometric effects, Collier and Hendry Counties, Florida* (No. 3). US
511 Department of the Interior, US Geological Survey.

512 Moench, A. F. (1985). Transient flow to a large-diameter well in an aquifer with storative semiconfining
513 layers. *Water Resources Research*, 21(8), 1121-1131.

514 Narasimhan, T. N., Kanehiro, B. Y., & Witherspoon, P. A. (1984). Interpretation of earth tide response
515 of three deep, confined aquifers. *Journal of Geophysical Research: Solid Earth*, 89(B3), 1913-1924.

516 Pacheco, F. A. L. (2013). Hydraulic diffusivity and macrodispersivity calculations embedded in a
517 geographic information system. *Hydrological sciences journal*, 58(4), 930-944.

518 Rabinovich, A., Barrash, W., Cardiff, M., Hochstetler, D. L., Bakhos, T., Dagan, G., & Kitanidis, P. K.
519 (2015). Frequency dependent hydraulic properties estimated from oscillatory pumping tests in an
520 unconfined aquifer. *Journal of Hydrology*, 531, 2-16.

521 [Rahi, K. A., & Halihan, T. \(2013\). Identifying aquifer type in fractured rock aquifers using harmonic](#)
522 [analysis. *Groundwater*, 51\(1\), 76-82.](#)

523 Renner, J., & Messar, M. (2006). Periodic pumping tests. *Geophysical Journal International*, 167(1), 479-
524 493.

525 Roeloffs, E. (1996). Poroelastic techniques in the study of earthquake-related hydrologic phenomena.
526 *Advances in geophysics*, 37, 135-195. [https://doi.org/10.1016/S0065-2687\(08\)60270-8](https://doi.org/10.1016/S0065-2687(08)60270-8)

527 Rojstaczer, S., & Agnew, D. C. (1989). The influence of formation material properties on the response
528 of water levels in wells to Earth tides and atmospheric loading. *Journal of Geophysical Research:*
529 *Solid Earth*, 94(B9), 12403-12411.

530 Sedghi, M. M., & Zhan, H. (2016). Hydraulic response of an unconfined-fractured two-aquifer system
531 driven by dual tidal or stream fluctuations. *Advances in water resources*, 97, 266-278.

532 Schweizer, D., Ried, V., Rau, G. C., Tuck, J. E., & Stoica, P. (2021). Comparing Methods and Defining
533 Practical Requirements for Extracting Harmonic Tidal Components from Groundwater Level
534 Measurements. *Mathematical Geosciences*, 1-23.

535 Shen, Q., Zheming, S., Guangcai, W., Qingyu, X., Zejun, Z., & Jiaqian, H. (2020). Using water-level
536 fluctuations in response to Earth-tide and barometric-pressure changes to measure the in-situ
537 hydrogeological properties of an overburden aquifer in a coalfield. *Hydrogeology Journal*, 1-15.

538 Sun, X., Shi, Z., Xiang, Y (2020). Frequency dependence of in-situ transmissivity estimation of well-
539 aquifer systems from periodic loadings. *Water Resources Research*, e2020WR027536.

540 Valois, R., Vouillamoz, J. M., Lun, S., & Arnout, L. (2017). Assessment of water resources to support the
541 development of irrigation in northwest Cambodia: a water budget approach. *Hydrological Sciences*
542 *Journal*, 62(11), 1840-1855.

543 Valois, R., Vouillamoz, J. M., Lun, S., & Arnout, L. (2018). Mapping groundwater reserves in
544 northwestern Cambodia with the combined use of data from lithologies and time-domain-
545 electromagnetic and magnetic-resonance soundings. *Hydrogeology Journal*, 26(4), 1187-1200.

546 Valois, R., Rau, G. C., Vouillamoz, J. M., & Derode, B. (2022). Estimating hydraulic properties of the
547 shallow subsurface using the groundwater response to Earth and atmospheric tides: a comparison
548 with pumping tests. *Water Resources Research*, 58(5), e2021WR031666.

549 Van Everdingen, A. F. (1953). The skin effect and its influence on the productive capacity of a well.
550 *Journal of petroleum technology*, 5(06), 171-176.

551 Vouillamoz, J. M., Sokheng, S., Bruyere, O., Caron, D., & Arnout, L. (2012). Towards a better estimate of
552 storage properties of aquifer with magnetic resonance sounding. *Journal of Hydrology*, 458, 51-58.

553 Vouillamoz, J. M., Valois, R., Lun, S., Caron, D., & Arnout, L. (2016). Can groundwater secure drinking-
554 water supply and supplementary irrigation in new settlements of North-West
555 Cambodia? *Hydrogeology Journal*, 24(1), 195-209.

556 Wang, C. Y., Doan, M. L., Xue, L., & Barbour, A. J. (2018). Tidal response of groundwater in a leaky
557 aquifer—Application to Oklahoma. *Water Resources Research*, 54(10), 8019-
558 8033. <https://doi.org/10.1029/2018WR022793>

559 Wang, H. F. (2000). *Theory of linear poroelasticity with applications to geomechanics and*
560 *hydrogeology* (Vol. 2). Princeton University Press.

561 [Wen, Z., Zhan, H., Huang, G., & Jin, M. \(2011\). Constant-head test in a leaky aquifer with a finite-](#)
562 [thickness skin. *Journal of Hydrology*, 399\(3-4\), 326-334.](#)

563 Young, A. (1913). Tidal phenomena at inland boreholes near Cradock. *Transactions of the Royal Society*
564 *of South Africa*, 3(1), 61-106.

565 Zhang, H., Shi, Z., Wang, G., Sun, X., Yan, R., & Liu, C. (2019a). Large earthquake reshapes the
566 groundwater flow system: Insight from the water-level response to earth tides and atmospheric
567 pressure in a deep well. *Water Resources Research*, 55(5), 4207-4219.

568 Zhang, S., Shi, Z., & Wang, G. (2019b). Comparison of aquifer parameters inferred from water level
569 changes induced by slug test, earth tide and earthquake—A case study in the three Gorges
570 area. *Journal of Hydrology*, 579, 124169.

571

572 Appendix

573 Appendix A: The analytical solution in the aquitard

574 To solve Equation 14 with the boundary conditions in Equations 7 and 8, we define:

$$575 \quad \widehat{h}_0 = h'_0 - \frac{B'K'_u}{\rho g} \varepsilon_0 \quad (\text{A1})$$

576 Thus, the equation system become:

$$577 \quad \left(\frac{\partial^2 \widehat{h}_0}{\partial z^2} \right) = \frac{i\omega \widehat{h}_0}{D'} \quad (\text{A2})$$

$$578 \quad \widehat{h}_0(z = z_i) = h_0 - \frac{B'K'_u}{\rho g} \varepsilon_0 \quad (\text{A3})$$

$$579 \quad \widehat{h}_0(z = 0) = h'_j - \frac{B'K'_u}{\rho g} \varepsilon_0 \quad (\text{A4})$$

580 The solution \widehat{h}_0 is of the form:

$$581 \quad \widehat{h}_0 = A_1 e^{\frac{(1+i)}{\delta}(z-z_i)} + A_2 e^{-\frac{(1+i)}{\delta}(z-z_i)} \quad (\text{A5})$$

582 It yields

$$583 \quad A_1 = \frac{e^{\frac{(1+i)}{\delta}z_i} \left(h_0 - \frac{B'K'_u}{\rho g} \varepsilon_0 \right) - \left(h'_j - \frac{B'K'_u}{\rho g} \varepsilon_0 \right)}{2 \sinh \left(\frac{(1+i)}{\delta} z_i \right)} \quad (\text{A6})$$

$$584 \quad A_2 = \frac{-e^{-\frac{(1+i)}{\delta}z_i} \left(h_0 - \frac{B'K'_u}{\rho g} \varepsilon_0 \right) + \left(h'_j - \frac{B'K'_u}{\rho g} \varepsilon_0 \right)}{2 \sinh \left(\frac{(1+i)}{\delta} z_i \right)} \quad (\text{A7})$$

585

586 Thus:

$$587 \quad h'_0 = A_1 e^{\frac{(1+i)}{\delta}(z-z_i)} + A_2 e^{-\frac{(1+i)}{\delta}(z-z_i)} + \frac{B'K'_u}{\rho g} \varepsilon_0 \quad (\text{A8})$$

588

589 Appendix B: Additional information on parameter exploration

590

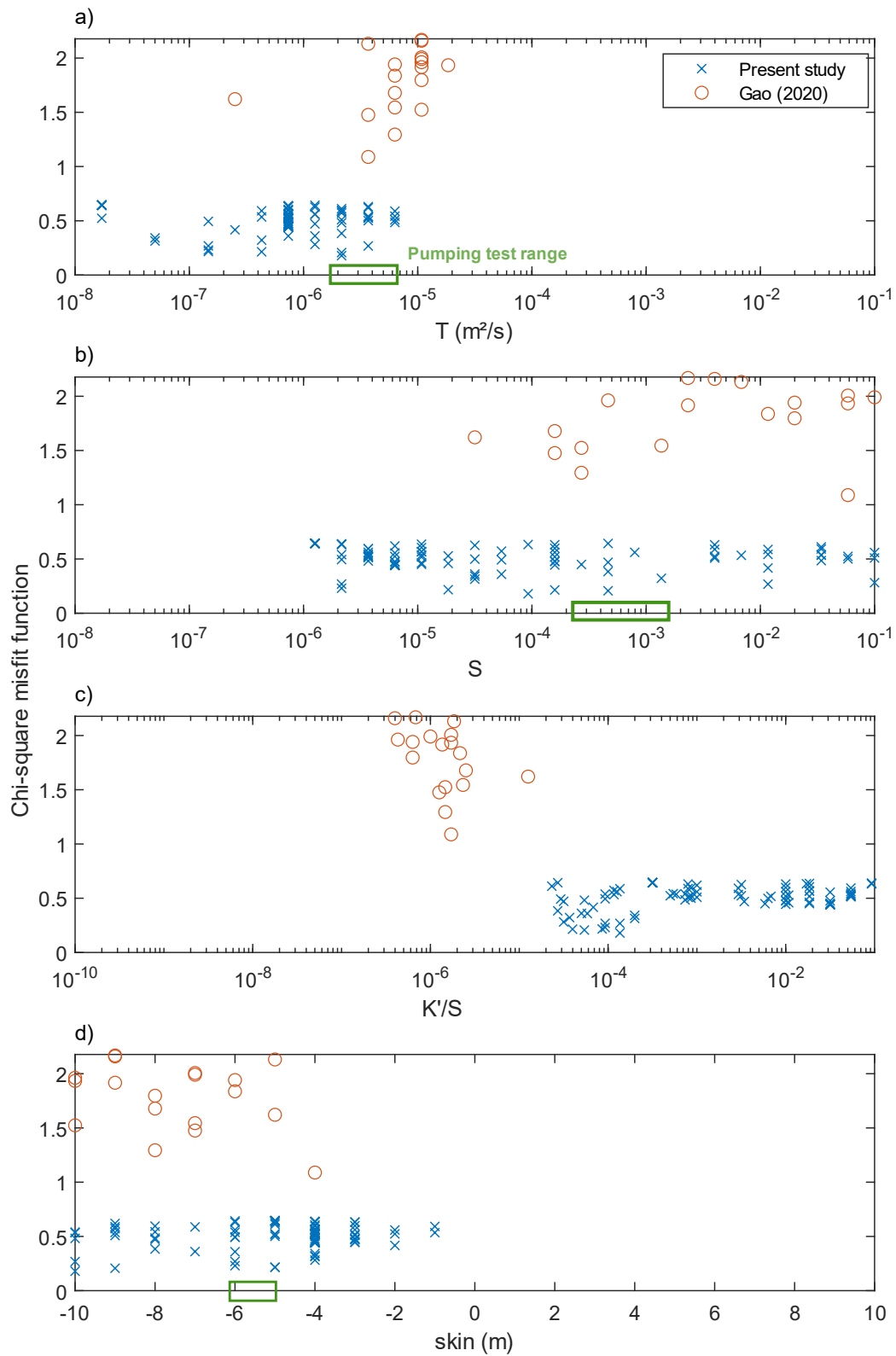
591 The figure A1 shows the misfit functions using the model developed in this study and the model of
592 Gao et al . (2020). Misfits are clearly higher for the older model that do not consider storage and
593 tidal response in the aquitard. Storativity best-fit using the model of Gao et al (2020) failed to
594 reproduce pumping test values. Nevertheless, transmissivity and skin estimates fall within
595 pumping test range.

596

597

598

599



600

601 *Figure A1: Comparison of misfit function for the present model and the one of Gao et al. (2020) for the Cambodian case study.*
 602 *Only the first hundred best-fit were plotted.*

603